# High-temperature conductivity of one-dimensional electrons

O. Entin-Wohlman
*The Racah Institute of Physics, Jerusalem 91904, Israel*
*and School of Physics and Astronomy, Tel Aviv University, Tel Aviv 69978, Israel**
(Received 25 July 1984)

The inelastic phonon scattering of one-dimensional electrons is analyzed by a diagrammatic technique. The contribution of the maximally crossed diagrams is evaluated for $\omega_{ph}\tau_{ph} \gg 1$ and $\omega_{ph}\tau_{ph} \ll 1$, where $\omega_{ph}$ and $\tau_{ph}$ are the phonon frequency and the inelastic relaxation time, respectively. The dependence of the conductivity upon $\omega_{ph}$ and $\tau_{ph}$ is found. In the $\omega_{ph}\tau_{ph} \ll 1$ limit, the scaling result of Abrikosov and Ryzhkin is reproduced.

## I. INTRODUCTION

Electronic conduction in one-dimensional disordered systems has attracted considerable interest in recent years. In the case of static disorder, Mott and Twose[1] argued that all electronic states are localized and consequently the dc conductivity vanishes. Later Mott[2] showed that the frequency-dependent conductivity is proportional to $\omega^2(\ln\omega)^2$ at low frequencies. These results are supported by rigorous diagrammatic treatments of the elastic scattering of the electrons from static impurities.[3-5]

Dynamic disorder destroys the strong interference effects which in the case of static disorder leads to localization. This kind of disorder may arise from the electron-phonon interaction. At temperatures higher than the characteristic phonon frequency the quantum effects of the phonons (e.g., the Peierls transition) may be neglected, and the main effect is the inelastic scattering of the electrons.

In considering the electronic conduction in the presence of dynamic disorder alone, one can distinguish between two regimes. The first is the regime of strong inelasticity, where $\omega_{ph}\tau_{ph} \gg 1$. Here $\omega_{ph}$ and $\tau_{ph}$ are the typical phonon frequency and inelastic electronic relaxation time, respectively. In this regime the leading term of the conductivity is proportional to $\tau_{ph}$ and does not depend explicitly upon $\omega_{ph}$.[4,6] This is the usual result of the Boltzmann equation. The situation in the weak-inelasticity regime, $\omega_{ph}\tau_{ph} \ll 1$, is much less clear. The diagrammatic approach of Gogolin, Melnikov, and Rashba[6] fails in this region. The scaling approach of Abrikosov and Ryzhkin[4] yields a conductivity linear in $\omega_{ph}$ and quadratic in $\tau_{ph}$, while Madhukar and Cohen[7] obtain a quadratic dependence upon $\omega_{ph}$.

The aim of this paper is to study the phonon-induced conductivity of one-dimensional electrons by a diagrammatic technique similar to that of Vollhardt and Wölfle.[5] They have developed this technique to study the elastic scattering of electrons by static impurities. In particular, they have pointed out the important role played by a special class of diagrams, the maximally crossed diagrams, which in $d < 2$ lead to the Anderson localization. We extend their method to the case of inelastic scattering. We show that the sum of the maximally crossed diagrams is important in the $\omega_{ph}\tau_{ph} \ll 1$ limit and evaluate its contribution to the conductivity. In the strong inelasticity regime ($\omega_{ph}\tau_{ph} \gg 1$) we find the correction to the Boltzmann-equation result. In the weak-inelasticity regime we reproduce the scaling result of Abrikosov and Ryzhkin.[4]

The system we consider is that of one-dimensional electrons interacting with three-dimensional phonons. This corresponds, for example, to organic metals like tetrathiafulvalene tetracyanoquinoclimethane (TTF-TCNQ). These quasi-one-dimensional materials in which the electronic conduction is along the chains have a relatively high conductivity that obeys a $T^{-2}$ law at high temperatures.[8] The $\tau_{ph}^2$ dependence of the calculated conductivity in the weak-inelasticity regime reproduces this temperature behavior since $\tau_{ph} \propto 1/T$ for a linear electron-phonon coupling. An alternative explanation to the $T^{-2}$ law is based upon a quadratic electron-phonon coupling in conjunction with the first Born approximation for the inelastic relaxation rate.[9,10] The two expressions for the conductivity differ in their dependence upon $\omega_{ph}$. Thus, the question of whether the prominent electron-phonon interaction in organic metals is linear or quadratic in the phonon operators should be determined by probing experimentally the phonon frequency dependence of the

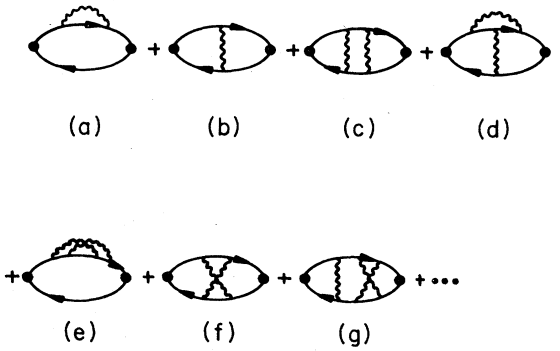


FIG. 1. Diagrammatic representation of the conductivity bubbles [Eq. (2.2)]. The upper solid line is the retarded electron line and the lower solid line is the advanced electron line. The wavy lines represent phonon insertions.

 

conductivity and other properties related to the electron-phonon interaction.

## II. METHOD OF CALCULATION

We consider a system of noninteracting electrons with energy spectrum $\xi_p$ measured from the Fermi energy

$$\xi_p=\frac{p^2}{2m}-\epsilon_F \ . \tag{2.1}$$

In the weak scattering limit the conductivity is determined by the electrons at the vicinity of $\pm p_F$, i.e., by the states with momenta $p=p_F+k$ and $p=-p_F+k$, where $k \ll p_F$. Therefore, following Abrikosov and Ryzhkin[4] we write the free-electron energy as $vk\sigma_3$, where $v$ is the Fermi velocity and $\sigma_i$ $(i=1,2,3)$ are the Pauli matrices. Accordingly, the single-particle Green's function $G_p$ is a $2\times 2$ diagonal matrix, in which the 11 and 22 entries correspond to $p=p_F+k$ and $p=-p_F+k$, respectively. In these notations, the wave-vector- and frequency-dependent conductivity is given by[4,11]

$$\sigma(q,\omega)=\frac{2e^2v^2}{S}\int\frac{d\epsilon}{2\pi}\left[-\frac{\partial f}{\partial\epsilon}\right]\sum_p \mathrm{Tr}\langle\sigma_3 G_p^R(\epsilon)\sigma_3 G_{p-q}^A(\epsilon-\omega)\rangle \ . \tag{2.2}$$

Here $S$ is the cross-section area of the unit cell perpendicular to the chain on which the electrons are moving, $f(\epsilon)$ is the Fermi function, and $G^R$ and $G^A$ are the retarded and advanced Green's functions, respectively. The angular brackets in Eq. (2.2) denote all possible phonon insertions into the electron-hole bubble (see Fig. 1).

We now denote

$$\Pi_{p,\epsilon}(q,\omega)=\langle G_p^R(\epsilon)\sigma_3 G_{p-q}^A(\epsilon-\omega)\rangle \tag{2.3}$$

and construct an equation for $\Pi$ in terms of the single-particle Green's functions and the irreducible vertex part. The derivation extends that of Vollhardt and Wölfle[5] to the case of inelastic scattering. (Note that each phonon line in Fig. 1 changes the energies of the particle and hole lines.)

We rewrite Eq. (2.3) in the form

$$\Pi_{p,\epsilon}(q,\omega)=G_p^R(\epsilon)\sigma_3 G_{p-q}^A(\epsilon-\omega)+\int d\epsilon_1\sum_{p_1} G_p^R(\epsilon)\Gamma_{pp_1}(\epsilon\epsilon_1)G_{p_1}^R(\epsilon_1)\sigma_3 G_{p_1-q}^A(\epsilon_1-\omega)\Gamma_{p_1p}(\epsilon_1\epsilon)G_{p-q}^A(\epsilon-\omega) \ . \tag{2.4}$$

Here $G_p$ denotes the single-particle Green's function which includes all self-energy insertions [e.g., diagrams (a) and (e) in Fig. 1]. The notation $\Gamma_{pp_1}(\epsilon\epsilon_1)X_{p_1\epsilon_1}(q,\omega)\Gamma_{p_1p}(\epsilon_1\epsilon)$ stands for all insertion of phonon lines between the particle and the hole lines [e.g., diagrams (b), (c), (d), (f), and (g) in Fig. 1]. In the matrix notations introduced above the electron-phonon vertices, and consequently $\Gamma$, are matrices. The explicit expressions for them are given in the next section. The vertex function $\Gamma$ includes reducible [diagrams (c) and (g) in Fig. 1] and irreducible [diagrams (b), (d), and (f)] contributions. Denoting the irreducible vertex function by $U$ we have

$$\begin{aligned}\int d\epsilon_1\sum_{p_1}\Gamma_{pp_1}(\epsilon\epsilon_1)G_{p_1}^R(\epsilon_1)\sigma_3 G_{p_1-q}^A(\epsilon_1-\omega)\Gamma_{p_1p}(\epsilon_1\epsilon)&\\ =\int d\epsilon_1\sum_{p_1}U_{pp_1}(\epsilon\epsilon_1)G_{p_1}^R(\epsilon_1)\sigma_3 G_{p_1-q}^A(\epsilon_1-\omega)U_{p_1p}(\epsilon_1\epsilon)&\\ +\int d\epsilon_1 d\epsilon_2\sum_{p_1,p_2}U_{pp_1}(\epsilon\epsilon_1)G_{p_1}^R(\epsilon_1)\Gamma_{p_1p_2}(\epsilon_1\epsilon_2)G_{p_2}^R(\epsilon_2)\sigma_3 G_{p_2-q}^A(\epsilon_2-\omega)\Gamma_{p_2p_1}(\epsilon_2\epsilon_1)G_{p_1-q}^A(\epsilon_1-\omega)U_{p_1p}(\epsilon_1\epsilon) \ .&\end{aligned} \tag{2.5}$$

Inserting Eq. (2.5) into Eq. (2.4), we obtain $\Pi$ in terms of the irreducible vertex function $U$:

$$\Pi_{p,\epsilon}(q,\omega)=G_p^R(\epsilon)\sigma_3 G_{p-q}^A(\epsilon-\omega)+\int d\epsilon_1\sum_{p_1}G_p^R(\epsilon)U_{pp_1}(\epsilon\epsilon_1)\Pi_{p_1,\epsilon_1}(q,\omega)U_{p_1p}(\epsilon_1\epsilon)G_{p-q}^A(\epsilon-\omega) \ . \tag{2.6}$$

The integral equation (2.6) for $\Pi$ is solved as follows. The Green's function $G_p^{R(A)}$ is given by

$$G_p^{R(A)}(\epsilon)=[\epsilon-vk\sigma_3-\Sigma_p^{R(A)}(\epsilon)]^{-1} \ , \tag{2.7}$$

where the self-energy part $\Sigma^{R(A)}$ is a $2\times 2$ diagonal matrix. The matrix $U\Pi U$ is also diagonal, since scattering by the phonons affects only the electron states with $p$ at the vicinity of $\pm p_F$. We therefore rewrite Eq. (2.6) in the form

$$[-\omega+\Sigma_p^R(\epsilon)-\Sigma_{p-q}^A(\epsilon-\omega)+vq\sigma_3]\Pi_{p,\epsilon}(q,\omega)=\Delta G_{p,\epsilon}(q,\omega)\left[\sigma_3+\int d\epsilon_1\sum_{p_1}U_{pp_1}(\epsilon\epsilon_1)\Pi_{p_1,\epsilon_1}(q,\omega)U_{p_1p}(\epsilon_1\epsilon)\right] \ , \tag{2.8}$$

where

$$\Delta G_{p,\epsilon}(q,\omega)=G_p^R(\epsilon)-G_{p-q}^A(\epsilon-\omega) \ . \tag{2.9}$$

Using the Ward identity (the proof is given in Appendix A)

$$\Sigma^R_p(\epsilon)-\Sigma^A_{p-q}(\epsilon-\omega)=\int d\epsilon_1 \sum_{p_1} U_{pp_1}(\epsilon\epsilon_1)\Delta G_{p_1,\epsilon_1}(q,\omega)U_{p_1p}(\epsilon_1\epsilon)\ , \tag{2.10}$$

we obtain from (2.8)

$$(-\omega+vq\sigma_3)\Pi_{p,\epsilon}(q,\omega)=\Delta G_{p,\epsilon}(q,\omega)\sigma_3+\int d\epsilon_1 \sum_{p_1}[\Delta G_{p,\epsilon}(q,\omega)U_{pp_1}(\epsilon\epsilon_1)\Pi_{p_1,\epsilon_1}(q,\omega)U_{p_1p}(\epsilon_1\epsilon)$$
$$-U_{pp_1}(\epsilon\epsilon_1)\Delta G_{p_1,\epsilon_1}(q,\omega)U_{p_1p}(\epsilon_1\epsilon)\Pi_{p,\epsilon}(q,\omega)]\ . \tag{2.11}$$

Making the ansatz

$$\Pi_{p,\epsilon}(q,\omega)=\Delta G_{p,\epsilon}(q,\omega)\eta(q,\omega)\ , \tag{2.12}$$

where $\eta$ is a $2\times 2$ matrix, we find from (2.11)

$$(-\omega+vq\sigma_3)\eta(q,\omega)=\sigma_3+M(q,\omega)\ , \tag{2.13}$$

where

$$M(q,\omega)=iv\int d\epsilon\, d\epsilon_1\left[-\frac{\partial f}{\partial\epsilon}\right]\sum_{pp_1}[\Delta G_{p,\epsilon}(q,\omega)U_{pp_1}(\epsilon\epsilon_1)\Delta G_{p_1,\epsilon_1}(q,\omega)\eta U_{p_1p}(\epsilon_1\epsilon)$$
$$-U_{pp_1}(\epsilon\epsilon_1)\Delta G_{p_1,\epsilon_1}(q,\omega)U_{p_1p}(\epsilon_1\epsilon)\Delta G_{p,\epsilon}(q,\omega)\eta]\ . \tag{2.14}$$

Inserting Eqs. (2.3), (2.7), and (2.12) into (2.2), we obtain

$$\sigma(q,\omega)=\frac{e^2v}{\pi S}(-i)\mathrm{Tr}(\sigma_3\eta(q,\omega))\ . \tag{2.15}$$

Thus, solving Eqs. (2.13) and (2.14) for $\eta$ and inserting the result into (2.15) gives an expression for the conductivity. In the next section we investigate various contributions to $M(q,\omega)$ and $\sigma(q,\omega)$.

## III. THE CALCULATION OF THE CONDUCTIVITY

Since we consider electronic states at the vicinity of $\pm p_F$, we shall distinguish between two phonon processes. In the first, an electron initially at the vicinity of $p_F$ $(-p_F)$ remains close to $p_F$ $(-p_F)$ after the emission or absorption of a phonon. This corresponds to forward scattering. The second process takes an electron from the vicinity of $p_F$ $(-p_F)$ to the vicinity of $-p_F$ $(p_F)$ and corresponds to backward scattering. The electron-phonon interaction is written accordingly in a matrix form[4]

$$H_{e\text{-ph}}=\sum_{k_1k_2}[g(k_1-k_2)\varphi_{k_1-k_2}\psi^\dagger_{k_1}\psi_{k_2}+g(2p_F+k_1-k_2)\varphi_{2p_F+k_1-k_2}\tfrac{1}{2}\psi^\dagger_{k_1}(\sigma_1+i\sigma_2)\psi_{k_2}$$
$$+g(-2p_F+k_1-k_2)\varphi_{-2p_F+k_1-k_2}\tfrac{1}{2}\psi^\dagger_{k_1}(\sigma_1-i\sigma_2)\psi_{k_2}]\ , \tag{3.1}$$

where $g$ denotes the electron-phonon matrix element,

$$\varphi_k=b_k+b^\dagger_{-k}\ , \tag{3.2}$$

$b$ and $b^\dagger$ are the phonon operators, and

$$\psi_k=\begin{bmatrix}c_{p_F+k}\\ c_{-p_F+k}\end{bmatrix},\quad \psi^\dagger_k=(c^\dagger_{p_F+k},\ c^\dagger_{-p_F+k})\ , \tag{3.3}$$

where $c$ and $c^\dagger$ are the electron operators. Equation (3.1) describes the interaction of one-dimensional electrons with three-dimensional phonons. For convenience the dependence of $g$ and $\varphi$ upon the transverse components of the momentum is suppressed. The first term in (3.1) describes forward scattering and the last two terms give the backward scattering.

Now consider a phonon line insertion, as depicted in Fig. 2. We denote the right-hand side of the diagram by $X_{p_1p'+p_1-p}(\epsilon_1\epsilon'+\epsilon_1-\epsilon)$ where $X$ is some $2\times 2$ matrix. In the high-temperature limit, where $T$ is larger than any typical phonon frequency, one obtains

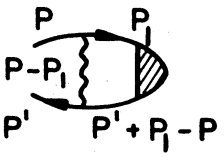


FIG. 2. Insertion of a phonon line. The shaded area is denoted $X_{p_1,p'+p_1-p}$ in the text. (Energy indices are suppressed for convenience.)

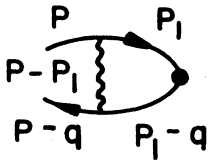


FIG. 3. Lowest-order contribution to $M(q,\omega)$ [Eq. (3.9)]. Energy indices are suppressed.

$$|g_1|^2\frac{T}{\omega_1}[\delta(\epsilon-\epsilon_1-\omega_1)+\delta(\epsilon-\epsilon_1+\omega_1)]X_{p_1p'+p_1-p}(\epsilon_1\epsilon'+\epsilon_1-\epsilon)$$
$$+|g_2|^2\frac{T}{\omega_2}[\delta(\epsilon-\epsilon_1-\omega_2)+\delta(\epsilon-\epsilon_1+\omega_2)]\tfrac{1}{2}(\sigma_1X_{p_1p'+p_1-p}\sigma_1+\sigma_2X_{p_1p'+p_1-p}\sigma_2)\ . \quad (3.4)$$

Here we have introduced the following notations. The matrix element for forward scattering is $g_1$ and the corresponding phonon frequency is $\omega_1$. (Note that $\omega_1$ includes the transverse momenta, and thus does not vanish even if the momentum transfer along the chain is small.) Similarly, $g_2$ and $\omega_2$ are the matrix element and phonon frequency for backward scattering, respectively. The factors $T/\omega_1$ and $T/\omega_2$ result from the phonon occupation numbers in the high-temperature limit.

To demonstrate this procedure we calculate in some detail the lowest-order contribution to the self-energy part $\Sigma^R_p(\epsilon)-\Sigma^A_{p-q}(\epsilon-\omega)$. In this case the matrix $X$ in Eq. (3.4) becomes $\Delta G_{p_1,\epsilon_1}(q,\omega)$ [see Eqs. (2.9) and (2.10)]. Summing over $p_1$ and integrating over $\epsilon_1$ we get

$$\Sigma^R_p(\epsilon)-\Sigma^A_{p-q}(\epsilon-\omega)=-\frac{i}{v}\left[2|g_1|^2\frac{T}{\omega_1}+2|g_2|^2\frac{T}{\omega_2}\right], \quad (3.5)$$

which is proportional to a unit matrix. Introducing the forward $(1/\tau_1)$ and backward $(1/\tau_2)$ scattering rates

$$\frac{1}{\tau_1}=\frac{2}{v}|g_1|^2\frac{T}{\omega_1},\quad \frac{1}{\tau_2}=\frac{2}{v}|g_2|^2\frac{T}{\omega_2}, \quad (3.6)$$

we find

$$\Sigma^R_p(\epsilon)-\Sigma^A_{p-q}(\epsilon-\omega)=-i\left[\frac{1}{\tau_1}+\frac{1}{\tau_2}\right]\equiv-\frac{i}{\tau}\ . \quad (3.7)$$

In the weak scattering limit and at high temperatures, the single-particle Green's functions are smoothly varying functions of the interaction, as in the case of elastic scattering. Therefore, we shall use for $\Sigma^R$ and $\Sigma^A$ (which enter the expressions for $G^R$ and $G^A$) the lowest-order result

$$\Sigma^R=-\Sigma^A=-\frac{i}{2\tau}\ . \quad (3.8)$$

Having constructed the expressions for $G^{R(A)}_p$ and consequently for $\Delta G$ [Eqs. (2.7) and (2.9)], we now turn to examine the matrix $M(q,\omega)$ [Eq. (2.14)]. The lowest-order contribution to it is depicted in Fig. 3. Carrying out the summations as indicated in Eqs. (3.4) and (3.6) we find

$$M^0(q,\omega)=-\frac{i}{\tau_2}[\sigma_1\eta(q,\omega)\sigma_1-\eta(q,\omega)]\ . \quad (3.9)$$

We now turn to examine the contribution of the maximally crossed diagrams (Fig. 4) to $M(q,\omega)$. In the case of elastic scattering these diagrams lead to the Anderson localization.[5] We show in Appendix B that the contribution of the maximally crossed (MC) diagrams to $M(q,\omega)$ is

$$M^{\mathrm{MC}}(q,\omega)=-\int d\epsilon_1\int\frac{dq_1}{2\pi}\{[-\epsilon_1-\omega-i/\tau+\sigma_3v(q_1-q)]^{-1}+[\epsilon_1-\omega-i/\tau-\sigma_3v(q_1-q)]^{-1}\}$$
$$\times K_{q_1-q}(\epsilon_1,\omega)[\sigma_1\eta(q,\omega)\sigma_1-\eta(q,\omega)]\ , \quad (3.10)$$

where

$$K_{q_1-q}(\epsilon_1,\omega)=\tfrac{1}{2}[L_{q_1-q}(\epsilon_1,\omega)-\sigma_3L_{q_1-q}(\epsilon_1,\omega)\sigma_3]\sigma_1\ , \quad (3.11)$$

FIG. 4. The series of the maximally crossed diagrams.

and $L$ represents the infinite series of the maximally cross diagrams. Explicitly,

$$L_{q_1-q}(\epsilon_1,\omega)=\int d\epsilon_2 F_{\epsilon_2} c_{q_1-q}(2\epsilon_2-\epsilon_1-\omega)F_{\epsilon_1-\epsilon_2}+\int d\epsilon_2 d\epsilon_3 F_{\epsilon_2} c_{q_1-q}(2\epsilon_2-\epsilon_1-\omega)F_{\epsilon_3-\epsilon_2}c_{q_1-q}(2\epsilon_3-\epsilon_1-\omega)F_{\epsilon_1-\epsilon_3}+\cdots , \tag{3.12}$$

where

$$c_q(\epsilon)=-\frac{i}{v}\left[\epsilon-\frac{i}{\tau}+\sigma_3 vq\right]^{-1} \tag{3.13}$$

and

$$F_\epsilon=\frac{v}{2\tau_1}[\delta(\epsilon-\omega_1)+\delta(\epsilon+\omega_1)]+\sigma_1\frac{v}{2\tau_2}[\delta(\epsilon-\omega_2)+\delta(\epsilon+\omega_2)] . \tag{3.14}$$

The infinite series of (3.12) can be easily summed over in the case $\omega_1=\omega_2=0$ (i.e., elastic scattering). In that case the $\epsilon_i$ integrations yield the factor $\delta(\epsilon_1)$ and from Eqs. (3.11) and (3.12) we find

$$L_{q_1-q}(\epsilon_1,\omega)=\delta(\epsilon_1)\frac{v}{\tau_2}\frac{2i\omega/\tau_1-1/\tau^2}{\omega^2-v^2(q_1-q)^2+2i\omega/\tau_2},\quad \omega_1=\omega_2=0 . \tag{3.15}$$

Inserting this into Eq. (3.10) we obtain (in the small-$\omega\tau$ limit)

$$M^{\mathrm{MC}}(0,\omega)=-\frac{i}{\tau}\left[\frac{i}{2\omega\tau_2}\right]^{1/2}[\sigma_1\eta(\omega)\sigma_1-\eta(\omega)],\quad \omega_1=\omega_2=0 . \tag{3.16}$$

This reproduces the result obtained by Vollhardt and Wölfle[5] and diverges as the external frequency $\omega$ tends to zero.

In the other extreme limit, where the phonon frequencies are much larger than $1/\tau$, the terms in the infinite series (3.12) are very small. The general term is of the order $(v/\tau_{\mathrm{ph}})(1/\omega_{\mathrm{ph}}\tau_{\mathrm{ph}})^n$, where $\omega_{\mathrm{ph}}$ and $\tau_{\mathrm{ph}}^{-1}$ denote typical phonon frequency and scattering rate, respectively. Thus in the limit $\omega_{\mathrm{ph}}\tau_{\mathrm{ph}}\gg 1$, the crossed diagrams can be neglected, as has also been pointed out by Abrikosov and Ryzhkin.[4] The leading contribution of (3.12) to $M^{\mathrm{MC}}$ is

$$M^{\mathrm{MC}}(0,0)=-\frac{i}{\tau}\frac{1}{\omega_1^2\tau_1\tau_2}(\sigma_1\eta\sigma_1-\eta),\quad \omega_{\mathrm{ph}}\tau_{\mathrm{ph}}\gg 1 . \tag{3.17}$$

This is a small correction to the first Born approximation, Eq. (3.9).

To obtain the contribution of the maximally crossed diagrams in the $\omega_{\mathrm{ph}}\tau_{\mathrm{ph}}\ll 1$ limit, one needs to estimate the infinite series of (3.12). This is carried out in Appendix C. It is shown there that in that limit

$$M^{\mathrm{MC}}(0,\omega)=\int\frac{dq_1}{2\pi}\left[\left[\omega+\frac{i}{\tau}-\sigma_3 vq_1\right]^{-1}+\left[\omega+\frac{i}{\tau}+\sigma_3 vq_1\right]^{-1}\right]K_{q_1}(\omega)[\sigma_1\eta(\omega)\sigma_1-\eta(\omega)] , \tag{3.18}$$

where

$$K_{q_1}(\omega)=\frac{v}{\tau_2\tau^2}\left[v^2q_1^2-\frac{2i\omega}{\tau_2}+\tau^2\left[\frac{\omega_2^2}{\tau_2^2}+\frac{\omega_1^2}{\tau_1\tau_2}\right]\right]^{-1} . \tag{3.19}$$

Inserting (3.19) into (3.18) we find

$$M^{\mathrm{MC}}(0,\omega)=-\frac{i}{\tau\tau_2}\left[\frac{\omega_2^2\tau^2}{\tau_2^2}+\frac{\omega_1^2\tau^2}{\tau_1\tau_2}-\frac{2i\omega}{\tau_2}\right]^{-1/2}[\sigma_1\eta(\omega)\sigma_1-\eta(\omega)],\quad \omega_{\mathrm{ph}}\tau_{\mathrm{ph}}\ll 1 . \tag{3.20}$$

Let us now investigate the expressions for the conductivity in the various regimes. To this end we insert $M$ into (2.13), solve for $\eta$, and insert the result into Eq. (2.15) for $\sigma$. The lowest-order contribution, i.e., the first Born approximation [Eq. (3.19)], gives

$$\sigma^0(\omega)=\frac{e^2v}{\pi S}\frac{2}{-i\omega+2/\tau_2} . \tag{3.21}$$

Taking into account the leading-order correction in the $\omega_{\mathrm{ph}}\tau_{\mathrm{ph}}\gg 1$ limit [Eq. (3.17)] we find

$$\sigma(\omega)=\frac{e^2v}{\pi S}\frac{2}{-i\omega+(2/\tau_2)(1+1/\omega_1^2\tau_1\tau)},\quad \omega_{\mathrm{ph}}\tau_{\mathrm{ph}}\gg 1 . \tag{3.22}$$

In the other extreme limit, $\omega_{\mathrm{ph}}\tau_{\mathrm{ph}}\ll 1$, Eq. (3.20) yields

$$\sigma(\omega)=\frac{e^2v}{\pi S}2\left\{-i\omega+\frac{2}{\tau_2}\left[1+\frac{1}{\tau}\left[\frac{\omega_2^2\tau^2}{\tau_2^2}+\frac{\omega_1^2\tau^2}{\tau_2\tau_1}-\frac{2i\omega}{\tau_2}\right]^{-1/2}\right]\right\}^{-1},\quad \omega_{\rm ph}\tau_{\rm ph}\ll 1\ . \tag{3.23}$$

To obtain the qualitative behavior of the conductivity as a function of $\omega_{\rm ph}\tau_{\rm ph}$, we set the external frequency $\omega$ equal to zero and denote $\sigma_0=e^2v\tau_2/\pi S$. Then, from (3.22) and (3.23)

$$\frac{\sigma}{\sigma_0}=\begin{cases}1-1/2(\omega_{\rm ph}\tau_{\rm ph})^2, & \omega_{\rm ph}\tau_{\rm ph}\gg 1\\ \omega_{\rm ph}\tau_{\rm ph}/\sqrt{2}, & \omega_{\rm ph}\tau_{\rm ph}\ll 1\ .\end{cases} \tag{3.24}$$

The schematic behavior of $\sigma/\sigma_0$ as a function of $\omega_{\rm ph}\tau_{\rm ph}$ is shown in Fig. 5.

## IV. DISCUSSION

We have extended the diagrammatic method of Vollhardt and Wölfle[5] for the calculation of the conductivity to the case of inelastic scattering. We have investigated the contribution of the maximally crossed diagrams to $\sigma$ and have shown that in the strong-inelasticity limit ($\omega_{\rm ph}\tau_{\rm ph}\gg 1$) it yields a correction of order $(\omega_{\rm ph}\tau_{\rm ph})^{-2}$ to $\sigma_0$, where $\sigma_0$ is the Boltzmann-equation result of the conductivity. In the weak-inelasticity limit ($\omega_{\rm ph}\tau_{\rm ph}\ll 1$) the dc conductivity is linear in $\omega_{\rm ph}$ and quadratic in $\tau_{\rm ph}$, thus decreasing with temperature as $T^{-2}$. Thus, in the small $\omega_{\rm ph}\tau_{\rm ph}$ limit we reproduce the scaling result of Abrikosov and Ryzhkin.[4]

In the case of elastic scattering the divergence of $K_{q_1}(\omega)$ [see Eq. (3.19)] at small external frequency $\omega$, which leads to the vanishing of the dc conductivity, is removed in the presence of time-reversal invariance breaking. Vollhardt and Wölfle[5] point out that this results from the replacement of $\omega$ by $\omega+i/\tau_s$, where $\tau_s$ is, e.g., the spin-flip scattering time. From Eq. (3.19) it is seen that in the weak-inelasticity regime the role of the time-reversal breaking rate is played by $\omega_{\rm ph}^2\tau_{\rm ph}$, and not $\tau_{\rm ph}^{-1}$ as might be conjectured.

A recent numerical study of Marianer, Hartzstein, and Weger[12] has yielded a diffusion coefficient proportional to $\omega_{\rm ph}^{1/2}$ at frequencies much less than $\tau_{\rm ph}^{-1}$. The model describes the time-dependent width of an initially localized wave packet using a tight-binding Hamiltonian with time-dependent on-site energies. This latter time dependence is characterized by a frequency $\omega_{\rm ph}$. It is assumed there that $\hbar/\tau_{\rm ph}$ is not much less than the bandwidth. In this respect the numerical model is different from the model studied here. Whether this is the reason for the discrepancy in the $\omega_{\rm ph}$ dependence of the diffusion constant is not yet clear to us. We hope to study this question in the near future.

## ACKNOWLEDGMENTS

The author is grateful to Professor Shlomo Alexander for extensive and fruitful discussions. This research was supported by grants from the National Council for Research and Development, Israel and Kernforschungszentrum, Karlsruhe (KfK), Germany.

## APPENDIX A: PROOF OF THE WARD IDENTITY

Here we prove the identity (2.10) used in the derivation of Eqs. (2.13)–(2.15) for the conductivity. The proof is analogous to that constructed by Vollhardt and Wölfle[5] for the case of elastic scattering, though care must be taken when averaging over the phonon lines.

Consider, for example, the retarded self-energy diagram shown in Fig. 6(a). Subtracting from it the advanced self-energy diagram we obtain

$$\begin{aligned}\Sigma_p^R(\epsilon)-\Sigma_{p-q}^A(\epsilon-\omega)=\int d\epsilon_2\int d\epsilon_3\sum_{p_2,p_3}\ &(u_{p-p_2}\Delta G_{p_2}u_{p-p_3}G^R_{p_2+p_3-p}u_{p-p_2}G^R_{p_3}u_{p-p_3}\\ &+u_{p-p_2}G^A_{p_2-q}u_{p-p_3}\Delta G_{p_2+p_3-p}u_{p-p_2}G^R_{p_3}u_{p-p_3}\\ &+u_{p-p_2}G^A_{p_2-q}u_{p-p_3}G^A_{p_2+p_3-p-q}u_{p-p_2}\Delta G_{p_3}u_{p-p_3})\ .\end{aligned} \tag{A1}$$

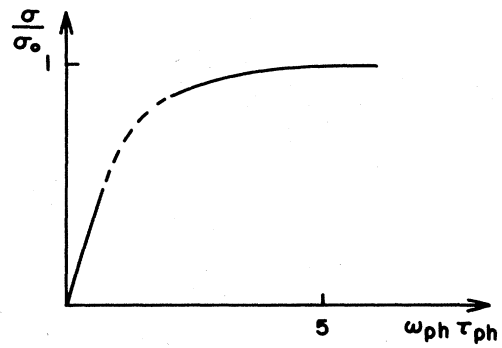


FIG. 5. The schematic dependence of the dc conductivity upon $\omega_{\rm ph}\tau_{\rm ph}$ [Eq. (3.24)].

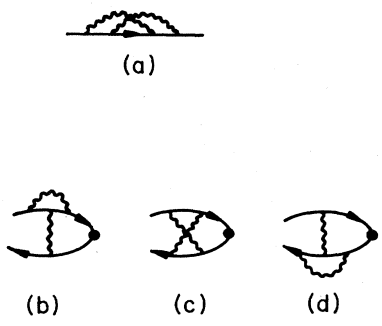


FIG. 6. Second-order irreducible diagrams. (a) Self-energy correction; (b), (c), and (d) irreducible vertex function.

Here $u_{p-p_2}$ denotes the electron-phonon vertex, $\Delta G$ is given by Eq. (2.9), and the energy indices are suppressed for convenience. Carrying out the phonon averaging according to Eq. (3.4), each term on the right-hand side of (A1) yields three terms. For example, the first term gives

$$A_{\epsilon-\epsilon_2}A_{\epsilon-\epsilon_3}\Delta G_{p_2}G^R_{p_2+p_3-p}G^R_{p_3}+A_{\epsilon-\epsilon_2}B_{\epsilon-\epsilon_3}\Delta G_{p_2}\sigma_1 G^R_{p_2+p_3-p}G^R_{p_3}\sigma_1+B_{\epsilon-\epsilon_2}A_{\epsilon-\epsilon_3}\sigma_1\Delta G_{p_2}G^R_{p_2+p_3-p}\sigma_1 G^R_{p_3}\ , \tag{A2}$$

where $A$ and $B$ refer to the forward and backward scattering (see text):

$$A_\epsilon=\frac{v}{2\tau_1}[\delta(\epsilon-\omega_1)+\delta(\epsilon+\omega_1)],\quad B_\epsilon=\frac{v}{2\tau_2}[\delta(\epsilon-\omega_2)+\delta(\epsilon+\omega_2)]\ . \tag{A3}$$

One can easily verify that (A2) is also the result of

$$\int d\epsilon_1\sum_{p_1}U_{pp_1}(\epsilon\epsilon_1)\Delta G_{p_1}U_{p_1p}(\epsilon_1\epsilon)\ , \tag{A4}$$

where $U$ here is depicted in Fig. 6(b). Similarly, the other two terms in (A1) give (A4) for $U$ of Figs. 6(c) and 6(d). In this way the Ward identity is proven diagram by diagram.

## APPENDIX B: CALCULATION OF THE MAXIMALLY CROSSED DIAGRAMS

Here we calculated in detail the first diagram of Fig. 4, and obtained the general term in the infinite series of the maximally crossed diagrams. From Eq. (2.14) we see that we need to consider

$$U_{pp_1}(\epsilon\epsilon_1)X_{p_1,\epsilon_1}U_{p_1p}(\epsilon_1\epsilon)\ , \tag{B1}$$

where $X_{p_1,\epsilon_1}$ is a diagonal matrix [$X_{p_1,\epsilon_1}=\Delta G_{p_1,\epsilon_1}\eta$ in the first member of $M(q,\omega)$, $X_{p_1,\epsilon_1}=\Delta G_{p_1,\epsilon_1}$ in the second member]. Using Eqs. (3.4) and (3.6) we find that for the first diagram of Fig. 4 expression (B1) is

$$\begin{aligned}\int d\epsilon_2\sum_{p_2}[&A_{\epsilon-\epsilon_2}A_{\epsilon_2-\epsilon_1}G^RX_{p_1,\epsilon_1}G^A+\tfrac{1}{2}A_{\epsilon-\epsilon_2}B_{\epsilon_2-\epsilon_1}(G^R\sigma_1X_{p_1,\epsilon_1}G^A\sigma_1+G^R\sigma_2X_{p_1,\epsilon_1}G^A\sigma_2)\\&+\tfrac{1}{2}B_{\epsilon-\epsilon_2}A_{\epsilon_2-\epsilon_1}(\sigma_1G^RX_{p_1,\epsilon_1}G^A+\sigma_2G^RX_{p_1,\epsilon_1}\sigma_2G^A)\\&+\tfrac{1}{4}B_{\epsilon-\epsilon_2}B_{\epsilon_2-\epsilon_1}(\sigma_1G^R\sigma_1X_{p_1,\epsilon_1}\sigma_1G^A\sigma_1+\sigma_1G^R\sigma_2X_{p_1,\epsilon_1}\sigma_1G^A\sigma_2+\sigma_2G^R\sigma_1X_{p_1,\epsilon_1}\sigma_2G^A\sigma_1+\sigma_2G^R\sigma_2X_{p_1,\epsilon_1}\sigma_2G^A\sigma_2)]\ ,\end{aligned} \tag{B2}$$

where

$$A_\epsilon=\frac{v}{2\tau_1}[\delta(\epsilon-\omega_1)+\delta(\epsilon+\omega_1)],\quad B_\epsilon=\frac{v}{2\tau_1}[\delta(\epsilon-\omega_2)+\delta(\epsilon+\omega_2)]\ , \tag{B3}$$

and

$$G^R=G^R_{p_2}(\epsilon_2),\quad G^A=G^A_{p+p_1-p_2-q}(\epsilon+\epsilon_1-\epsilon_2-\omega)\ . \tag{B4}$$

The last member of (B2) vanishes since $G^R$, $G^A$, and $X$ are diagonal matrices and for such matrices the combination in the brackets is identically zero. The first member vanishes upon integration with respect to $p_2$. Hence only the second and third members contribute. Carrying out the summation over $p_2$ we obtain

$$\sigma_1X_{p_1,\epsilon_1}\sigma_1\int d\epsilon_2[A_{\epsilon-\epsilon_2}B_{\epsilon_2-\epsilon_1}C_{k+k_1-q}(\epsilon+\epsilon_1-2\epsilon_2-\omega)+B_{\epsilon-\epsilon_2}A_{\epsilon_2-\epsilon_1\sigma_1}\sigma_1C_{k+k_1-q}(\epsilon+\epsilon_1-2\epsilon_2-\omega)\sigma_1]\ , \tag{B5}$$

where

$$\begin{aligned}C_{k+k_1-q}(\epsilon+\epsilon_1-2\epsilon_2-\omega)&=\sum_{p_2}G^R_{p_2}(\epsilon_2)\sigma_1G^A_{p+p_1-p_2-q}(\epsilon+\epsilon_1-\epsilon_2-\omega)\sigma_1\\&=-\frac{i}{v}\left[\epsilon+\epsilon_1-2\epsilon_2-\omega-\frac{i}{\tau}+v(k+k_1-q)\sigma_3\right]^{-1}\ .\end{aligned} \tag{B6}$$

Here we have used the notation $p=\pm p_F+k$ and $p_1=\pm p_F+k_1$.

In a similar way one can calculate the higher-order maximally crossed diagrams. We find it convenient to present their contribution to (B1) as follows:

$$U_{pp_1}(\epsilon\epsilon_1)X_{p_1,\epsilon_1}U_{p_1p}(\epsilon_1\epsilon)=\sigma_1X_{p_1,\epsilon_1}\sigma_1K_{k+k_1-q}(\epsilon-\epsilon_1,\omega)\ , \tag{B7}$$

where

$$K_{k+k_1-q}(\epsilon-\epsilon_1,\omega)=\tfrac{1}{2}[L_{k+k_1-q}(\epsilon-\epsilon_1,\omega)-\sigma_3 L_{k+k_1-q}(\epsilon-\epsilon_1,\omega)\sigma_3]\sigma_1 , \tag{B8}$$

and $L$ represents the infinite series,

$$L_{k+k_1-q}(\epsilon-\epsilon_1,\omega)=\int d\epsilon_2 F_{\epsilon-\epsilon_2} C(\epsilon+\epsilon_1-2\epsilon_2-\omega)F_{\epsilon_2-\epsilon_1} + \int d\epsilon_2 d\epsilon_3 F_{\epsilon-\epsilon_2} C(\epsilon+\epsilon_1-2\epsilon_2-\omega)F_{\epsilon_2-\epsilon_3} C(\epsilon+\epsilon_1-2\epsilon_3-\omega)F_{\epsilon_3-\epsilon_1}+\cdots . \tag{B9}$$

In Eq. (B9) all the matrices $C$ [see Eq. (B6)] depend upon $k+k_1-q$ and the matrix $F$ is given by

$$F_\epsilon=A_\epsilon+\sigma_1 B_\epsilon , \tag{B10}$$

where $A$ and $B$ are given by Eqs. (B3). One notes from Eq. (B8) that $K$ is a diagonal matrix. Therefore, inserting (B7) into Eq. (2.14) we obtain

$$M^{\mathrm{MC}}(q,\omega)=iv\int d\epsilon\, d\epsilon_1 \left[-\frac{\partial f}{\partial\epsilon}\right]\sum_{p,p_1}\Delta G_{p,\epsilon}\sigma_1\Delta G_{p_1,\epsilon_1}\sigma_1 K_{k+k_1-q}(\epsilon-\epsilon_1,\omega)[\sigma_1\eta(q,\omega)\sigma_1-\eta(q,\omega)] , \tag{B11}$$

where $p=\pm p_F+k$ and $p_1=\pm p_F+k_1$. Changing $k+k_1=q_1$ and using Eq. (2.9) we finally find Eq. (3.10).

## APPENDIX C: DERIVATION OF EQS. (3.18) AND (3.19)

In order to treat the infinite series (3.12) we write it in the form

$$L(\epsilon_1)=\int d\epsilon_2 F_{\epsilon_2} C(2\epsilon_2-\epsilon_1)P(\epsilon_1,\epsilon_2) , \tag{C1}$$

where

$$P(\epsilon_1,\epsilon_2)=F_{\epsilon_1-\epsilon_2}+\int d\epsilon_3 F_{\epsilon_3-\epsilon_2} C(2\epsilon_3-\epsilon_1)F_{\epsilon_1-\epsilon_3}+\cdots=F_{\epsilon_1-\epsilon_2}+\int d\epsilon_3 F_{\epsilon_3-\epsilon_2} C(2\epsilon_3-\epsilon_1)P(\epsilon_1,\epsilon_3) . \tag{C2}$$

Fourier transforming the energy variables, Eqs. (C1) and (C2) become

$$L(t)=2\pi\int dt_1 dt_2 F(t_1)C(t_2)P(t+t_2,t_1+2t_2) , \tag{C3}$$

$$P(t_1,t_2)=F(t_1)\delta(t_1-t_2)+2\pi F(t_2)\int dt_3 C(t_3)P(t_1+t_3,t_2+2t_3) . \tag{C4}$$

Here $C(t)$ is the Fourier transform of $C(\epsilon)$ [Eq. (3.13)] and $F(t)$ is the Fourier transform of $F(\epsilon)$ [Eq. (3.14)].

In the elastic scattering case $F(t)$ is a constant and consequently the function

$$\tilde{P}(t_1)=\int dt_2 P(t_1,t_2) \tag{C5}$$

is also a constant. Since, from Eqs. (C3) and (C4)

$$\tilde{P}(t)=F(t)+L(t) , \tag{C6}$$

it follows that in the elastic scattering case $L(t)$ is a constant and $L(\epsilon)\propto\delta(\epsilon)$.

To treat the inelastic case, we note that $C(t)$ decays to zero at $|t|\gtrsim\tau$. This implies [see Eqs. (3.10) and (3.13)] that we need $L(t)$ at times $|t|<\tau$ and hence, from (C3), $P(t_1,t_2)$ at times shorter than $\tau$. We accordingly replace $F(t)$ by $F(\tau)$ in Eq. (C4) and find

$$\tilde{P}(t_1)=F(\tau)+2\pi F(\tau)\int dt_3 C(t_3)\tilde{P}(t_1+t_3) . \tag{C7}$$

Solving for $\tilde{P}$ and inserting into (C6),

$$L(t)=L=[1-F(\tau)C]^{-1}F(\tau)CF(\tau) , \tag{C8}$$

where

$$C=2\pi\int dt\, C(t)=2\pi\frac{i}{v}\left[\omega+\frac{i}{\tau}-vq\sigma_3\right]^{-1} . \tag{C9}$$

Calculating $K$ from $L$ [see Eq. (3.11)], we obtain

$$K_{q_1}(\epsilon,\omega)=\delta(\epsilon)\frac{v}{\tau_2}\cos(\omega_2\tau)\left[\frac{2i(\omega+i/\tau)}{\tau_1}\cos(\omega_1\tau)-\left[\frac{\cos^2(\omega_2\tau)}{\tau_2^2}-\frac{\cos^2(\omega_1\tau)}{\tau_1^2}\right]\right] \times\left[(\omega+i/\pi)^2-v^2q_1^2-\frac{2i(\omega+i/\tau)}{\tau_1}\cos(\omega_1\tau)+\left[\frac{\cos^2(\omega_2\tau)}{\tau_2^2}-\frac{\cos^2(\omega_1\tau)}{\tau_1^2}\right]\right]^{-1} . \tag{C10}$$

In Eq. (3.19) we use the small-$\omega_1\tau,\omega_2\tau$ limit of this expression.

*Permanent address.
[1]N. F. Mott and W. D. Twose, Adv. Phys. **10**, 107 (1961).
[2]N. F. Mott, Philos. Mag. **22**, 7 (1970).
[3]V. L. Berezinsky, Zh. Eksp. Teor. Fiz. **65**, 1251 (1973) [Sov. Phys.—JETP **38**, 620 (1974)].
[4]A. A. Abrikosov and I. A. Ryzhkin, Adv. Phys. **27**, 147 (1978).
[5]D. Vollhardt and P. Wölfle, Phys. Rev. Lett. **45**, 842 (1980); Phys. Rev. B **22**, 4666 (1980).
[6]A. A. Gogolin, V. I. Melnikov, and E. I. Rashba, Zh. Eksp. Teor. Fiz. **69**, 327 (1975) [Sov. Phys.—JETP **42**, 168 (1975)].
[7]A. Madhukar and M. H. Cohen, Phys. Rev. Lett. **38**, 85 (1977).
[8]J. R. Cooper, D. Jerome, M. Weger, and S. Etemand, J. Phys. (Paris) Lett. **36**, L219 (1975).
[9]H. Gutfreund and M. Weger, Phys. Rev. B **16**, 1753 (1977).
[10]S. Marianer, V. Zevin, M. Weger, and D. Moses, J. Phys. C **15**, 3877 (1982).
[11]L. P. Gorkov and G. M. Eliashberg, Zh. Eksp. Teor. Fiz. **54**, 612 (1968) [Sov. Phys.—JETP **27**, 328 (1968)].
[12]S. Marianer, C. Hartzstein, and M. Weger, Solid State Commun. **43**, 695 (1982).